DNA Bases Assembled on the Au(110)/Electrolyte Interface: A Combined Experimental and Theoretical Study

ARTICLE *in* THE JOURNAL OF PHYSICAL CHEMISTRY B · JANUARY 2015

Impact Factor: 3.3 · DOI: 10.1021/jp511909f · Source: PubMed

4 AUTHORS, INCLUDING:

Princia Salvatore

Leibniz-Institut für Analytische Wissenschaften

8 PUBLICATIONS **41** CITATIONS

SEE PROFILE

Renat Nazmutdinov

Kazan National Research Technological Unive…

84 PUBLICATIONS **890** CITATIONS

SEE PROFILE

Jingdong Zhang

Technical University of Denmark

101 PUBLICATIONS **2,309** CITATIONS

SEE PROFILE

THE JOURNAL OF PHYSICAL CHEMISTRY B

Article

pubs.acs.org/JPCB

DNA Bases Assembled on the Au(110)/Electrolyte Interface: A Combined Experimental and Theoretical Study

Princia Salvatore,[†] Renat R. Nazmutdinov,[‡] Jens Ulstrup,[†] and Jingdong Zhang*[,†]

[†]Department of Chemistry, Building 207, Technical University of Denmark, 2800 Kongens Lyngby, Denmark

[‡]Kazan National Research Technological University, K. Marx Str., 68, 420015 Kazan, Republic of Tatarstan, Russian Federation

Supporting Information

ABSTRACT: Among the low-index single-crystal gold surfaces, the Au(110) surface is the most active toward molecular adsorption and the one with fewest electrochemical adsorption data reported. Cyclic voltammetry (CV), electrochemically controlled scanning tunneling microscopy (EC-STM), and density functional theory (DFT) calculations have been employed in the present study to address the adsorption of the four nucleobases adenine (A), cytosine (C), guanine (G), and thymine (T), on the Au(110)-electrode surface. Au(110) undergoes reconstruction to the (1 × 3) surface in electrochemical environment, accompanied by a pair of strong voltammetry peaks in the double-layer region in acid solutions. Adsorption of the DNA bases gives featureless voltammograms with lower double-layer capacitance, suggesting that all the bases are chemisorbed on the Au(110) surface. Further investigation of the surface structures of the adlayers of the four DNA bases by EC-STM disclosed lifting of the Au(110) reconstruction, specific molecular packing in dense monolayers, and pH dependence of the A and G adsorption. DFT computations based on a cluster model for the Au(110) surface were performed to investigate the adsorption energy and geometry of the DNA bases in different adsorbate orientations. The optimized geometry is further used to compute models for STM images which are compared with the recorded STM images. This has provided insight into the physical nature of the adsorption. The specific orientations of A, C, G, and T on Au(110) and the nature of the physical adsorbate/surface interaction based on the combination of the experimental and theoretical studies are proposed, and differences from nucleobase adsorption on Au(111)- and Au(100)-electrode surfaces are discussed.

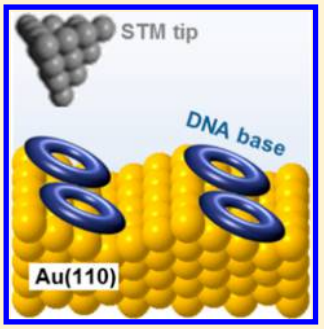

INTRODUCTION

Assembly of (bio)molecules on metal or other solid surfaces is an expanding interdisciplinary research field. Molecular targets range from individual biological building blocks, such as amino acids[1−3] and nucleobases,[4−14] to biological macromolecules, such as proteins, DNA (oligonucleotides), and whole biological cells.[15−22] Combined with metallic nanoparticles, biomolecules on solid surfaces provide potential applications in biological screening in the form of enzyme- and DNA-based "chips", biocompatible solid surfaces for medical implants, and monitoring and control of biofilms or other whole cell growth, within the general notion of biological surface science.[23,24]

The nature of the physical interaction between the (bio)molecules and the solid surface is crucial. The molecular interactions and two-dimensional surface packing raise issues regarding the nature of the binding, the need for well-defined substrate surfaces, and specific mechanisms of the formation of well-defined adlayers. Among all metals, gold is the most widely used substrate for molecular assembly because of its chemical inertness and biocompatibility. Gold is a relatively inert surface for DNA nucleobase adsorption, showing minimal specific molecule/gold interactions and promoting the formation of adsorbate layers through intermolecular forces.[9] An important property of the immobilized target (bio)molecules is their electronic conductivity. Together with the use of single-crystal, atomically planar metal surfaces, molecular conductivity is the basis for scanning tunneling microscopy (STM) that has enabled both structural mapping and functional control, even at the level of the single molecule.[15] Notably, this level of resolution now applies not only to ultrahigh vacuum (UHV) or ambient air environment, but also to fully functional bio-(macro)molecules directly in aqueous biological media via electrochemically controlled *in situ* STM (EC-STM).[25,26]

Linking biomolecular fragments, either as individual amino acids and nucleobases or as macro-biomolecular linking units, remains a challenge. Understanding of the substrate surface at the atomic level and mapping of the substrate−molecule interaction at least to molecular scale are crucial. This has been achieved for Au−S linked S-containing molecules that form highly ordered self-assembled molecular monolayers (SAMs) and for redox metalloproteins and metalloenzymes in aqueous solution under electrochemical control.[15,25,27] Au(111)-electrode surfaces have been by far the most commonly used substrate, but binding and single-molecule EC-STM mapping of a protein (human insulin) on Au(100) and Au(110) have also recently been reported.[28] On the other hand, pure and redox group modified oligonucleotides linked to polycrystalline Au-electrode surfaces have been extensively studied by

Received: December 1, 2014
Revised: January 20, 2015
Published: January 22, 2015

DOI: 10.1021/jp511909f
J. Phys. Chem. B 2015, 119, 3123−3134

electrochemical methods addressing long-range electron transfer along the double-strand axis.[22] Such studies have only recently been extended to single-crystal, i.e., Au(111), electrodes, EC-STM, and scanning tunneling spectroscopy.[20,21]

The individual nucleobases, adenine (A), cytosine (C), guanine (G), and thymine (T), as well as uracil (U), have long been voltammetric and STM targets supported by *in situ* infrared (IR) and surface-enhanced Raman spectroscopy.[4−14,29−39] A variety of substrates including highly oriented pyrolytic graphite (HOPG), MoS_2, Au, Ag, and Cu, have been used and showed base specific ordered two-dimensional patterns resolved to the single-molecule level.[40] Potential-dependent adsorbate phase transitions have further been mapped, and the interplay between substrate−adsorbate and adsorbate−adsorbate interactions clarified. Au(111)-electrode surfaces have mostly been used, but T and U adsorption on Au(100)-surfaces and A on Cu(110)-surfaces have also been studied.[8,29,30] Only a few studies of nucleobase adlayers at the Au(110)/liquid interface have however been reported so far.[12−14,33,41] These have focused on adenine, cytosine, and thymine adsorption and are based on spectroscopic methods, reflection anisotropy spectroscopy (RAS) in particular, but no single-molecule studies based on electrochemistry and *in situ* STM of the Au(110)-electrode surfaces have been reported so far. It is long recognized that the (110)-surface is the most open and most reactive of the three low-index electrochemical surfaces.[42−46] This offers more exclusive binding modes and therefore greater challenges for single-molecule STM image interpretation than the (111)- and (100)-surfaces. The (110) binding modes is also more likely to invoke symmetry breaking and chirality in the nucleobase molecular structure than on the more uniform (111)- and (100)-surfaces.[29] Adsorption-induced symmetry breaking has been conjectured to be involved in early stages of life evolution.[47,48]

In the present study adsorption of the four DNA nucleobases, A, G, C, and T, on Au(110)-electrode surfaces in aqueous buffers and acid solutions has been addressed using cyclic voltammetry (CV) and EC-STM. These techniques facilitate the formation of nucleobase adlayers under potential control. Primary views are to investigate the nucleobase/Au(110) adlayer structures in biological environment. Molecular scale features were observed, best for adenine. Structural images and packing interpretation are first offered and specific binding features of the four bases noted. This interpretation is compared with density functional theory (DFT) computations. This approach and molecular scale data such as these have not been reported before for Au(110). Submolecular resolution was not attained, but conclusions regarding packing, orientation and molecular surface interactions, and adsorption-induced nucleobase chirality in aqueous buffer can still be offered. Implications of the observations are discussed and compared with nucleobase adsorption on Au(111)- and Au(100)-electrode surfaces.

EXPERIMENTAL AND COMPUTATIONAL METHODS

Chemicals. The DNA bases adenine (A, 99%) and thymine (T, ≥99%) were from Sigma-Aldrich and cytosine (C, ≥99%) and guanine (G, ≥99%) from Fluka. Electrolyte solutions were prepared from KH_2PO_4 (99.99%), $NaClO_4$ (99.99%), $HClO_4$ (99.99%), and KOH (99.99%), all from Sigma-Aldrich, and ammonium acetate (NH_4Ac, 5 M solution, ultrapure for molecular biology), from Fluka. Other chemicals were highest purity and used without further purification. Millipore water (18.2 kΩ cm) was used throughout.

Electrochemistry. Cyclic voltammograms were recorded using a three-compartment cell and an electrochemical Autolab PGSTAT12 system controlled by the GPES software (Eco Chemie, Netherlands). A freshly in-house prepared reversible hydrogen electrode (RHE) and a Pt wire served as a reference and counter electrode, respectively. Electrolyte solutions were degassed with Ar (5 N) for 1 h and blanketed by Ar during the measurement.

In-house Au(110) bead electrodes (ca. 3 mm diameter), prepared from gold wires (<99.99%, 1 mm diameter, Goodfellow, England) according to Hamelin's method,[49] were used as working electrodes. The electrodes were annealed in a hydrogen flame prior to use, cooled in a hydrogen gas stream, and quenched in H_2-saturated water. The quality of the Au(110) electrodes was examined by CV in H_2SO_4 and $HClO_4$ and found to accord with reported voltammetric studies.[46,49]

The freshly annealed Au(110)-electrode was mounted in the electrochemical cell containing 0.1 M $NaClO_4/HClO_4$ (pH 2.5) as supporting electrolyte. A, C, and T were prepared in the same solution and introduced into the cell to give 0.4−10 mM concentrations. Alkaline solution (30 mM KOH, pH 12.0) was used for G due to its low solubility in acid and neutral media.

All potentials are reported against the saturated calomel electrode (SCE).

Scanning Tunneling Microscopy. Au(110) disc electrodes (SPL, The Netherlands) served as working electrodes for EC-STM. A PicoSPM *in situ* STM instrument (Agilent, USA) with a 3 mL Teflon in-house-built STM liquid cell and two platinum wires as counter and reference electrodes was used. The reference electrode was calibrated against a SCE after each experiment. Electrochemically etched W tips (0.25 mm diameter) coated with Apiezon wax were used as STM probes. EC-STM imaging in NH_4Ac (26 mM, pH 6.5) and $NaClO_4/HClO_4$ (0.1 M, pH 2.5) served to evaluate the reconstruction pattern of the Au(110) disc electrodes.

EC-STM was carried out using phosphate buffer (20 mM KH_2PO_4, pH 4.5), and acid (0.1 M $NaClO_4/HClO_4$, pH 2.5) and neutral (0.1 M NH_4Ac, pH 6.5) media as supporting electrolyte solutions. Nucleobase-modified Au(110)-electrode surfaces for EC-STM were prepared in two ways: *in situ* adsorption and pre-adsorption. In the former way, similar to electrochemical measurements, nucleobase solution was added to the STM cell (2−2.5 mL) in concentrations between 0.02 and 4 mM at a potential close to the open circuit potential (OCP). The surface structure was imaged by EC-STM at varying potential, in the presence of nucleobase in the STM cell. In the second procedure (pre-adsorption), the freshly annealed Au(110)-electrode surface was exposed for 5−18 h to (neutral or acid) electrolyte solution containing 0.5−10 mM nucleobase, rinsed in the same buffer to remove nonspecifically bound purine/pyrimidine molecules, mounted in the EC-STM cell, and scanned in nucleobase free electrolyte solution.

Low tunneling currents I_{tunnel} (30−100 pA) and bias voltages E_{bias} between −0.75 and 0.02 V were optimal for imaging and generally used. Substrate potentials E_w varied between −0.46 and 0.60 V vs SCE. All potentials are reported against a SCE.

Computational Method. Computational support based on a flexible and robust cluster model was achieved to describe theoretically the Au(110)-surface. Two-layer $Au_{32}(20 + 12)$, three-layer $Au_{44}(20 + 12 + 12)$, and four-layer $Au_{56}(20 + 12 + 12 + 12)$ clusters were used with the Au−Au bond lengths and

DOI: 10.1021/jp511909f
J. Phys. Chem. B 2015, 119, 3123−3134

symmetry corresponding to crystallographic data (fcc with the lattice constant a = 4.0788 Å). Surface reconstruction was neglected in accordance with the experimental observations. The electrode surface charge density was not included; i.e., potential of zero charge (PZC) conditions were assumed. This approximation is reasonable, as the surface charge density does not exceed ±5 μC cm^{-2} in the electrode potential region used in the experiments.[50] Adsorption of nucleobases in two different orientations, vertical and planar, was modeled. Protonated A and G were addressed as well. Several different Au(110)-surface sites were investigated, and selected positions, including the one of lowest adsorption energy, analyzed in detail. As the experimental data refer to the metal/solution interface, some information on the desorption energy of water molecules is desirable when describing the adsorption of DNA bases from solution bulk. Molecular dynamics simulations of a metal/solution interface would be needed to address this issue in the most appropriate way. However, in the present work, for the sake of simplicity, the analysis is restricted to a simplified approach where the desorption energy of one or two water molecules is taken into account. The adsorption of a single water molecule at different surface sites was therefore modeled as well, as presented in Figure S1 of the Supporting Information.

The quantum chemical calculations were performed at the DFT level using the M06-2X hybrid meta-functional with the kinetic energy density gradient as implemented in the Gaussian 09 program package.[51] Test calculations with other functionals (b3pw91, cam-b3lyp, and LC-wPBE)[51] were carried out for the T molecule. Here the computed adsorption energies (ranging from 0 to −0.09 eV) were found to be too small and are hardly suitable to describe chemisorption. The M06-2X functional that gives more reasonable results was therefore used instead (Tables 2−4 and Tables S1−S3). A similar meta-GGA functional (M06-L) predicts the adsorption energy of a benzene molecule at the Au(111) surface with good accuracy (error 5−10% as compared with experimental data[52]). The M06-2X functional also gives a reasonable adsorption energy for a water molecule adsorbed at Hg, Ga, and Bi(111) surfaces.[53] A basis set of double-ζ quality was employed to describe the valence electrons of the Au atoms, while the inner electrons were replaced by the effective core potentials developed by Hay and Wadt.[54] The standard triple-ζ 6-311g valence basis set augmented by polarization and diffuse functions was employed for the O, N, C, and H atoms. The geometry of the water molecules was optimized with symmetry constraints (two H atoms always with equal distance from the metal plane), while geometry optimization for the nucleobases was performed without restrictions. Solvent effects were addressed using the polarized continuum model (PCM)[51] with a value of 78 for the static dielectric constant (ε); spatial dispersion of ε in the vicinity of the electrode surface was disregarded. The calculated adsorption energies were corrected to the basis set superposition error (BSSE). Atomic charges were calculated using natural population analysis (NPA).[55]

RESULTS AND DISCUSSION

Reconstructed Au(110)-Electrode Surface. A cyclic voltammogram of the freshly annealed Au(110) surface is shown in Figure 1. Two anodic peaks at 1.0−1.15 V and one stronger cathodic peak at 0.78 V are apparent. These shoulders (peaks) come from multistep formation of a gold oxide layer (anodic peaks) and reduction of the gold oxide layer to gold

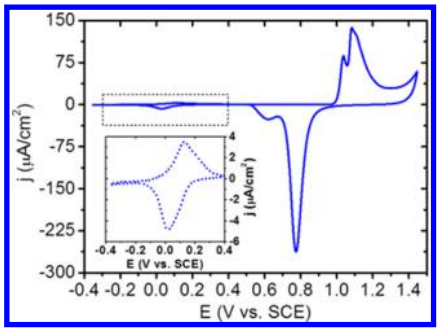

Figure 1. Cyclic voltammograms of bare Au(110)-electrode surface in 0.01 M H_2SO_4 (pH 2.0). Scan rate: 50 mV s^{-1}. The voltammetric peaks framed by the dashed rectangle is enlarged in the inset and represents the reconstruction signal in the double-layer region, between −0.4 and 0.4 V.

(cathodic peak). A pair of peaks at 0.0 and 0.15 V vs SCE in the double-layer region, consistent with reported observations for both $HClO_4$ and H_2SO_4,[44,45] is caused by reconstruction and lifting of reconstruction of the gold surface, respectively.

The Au(110)-surface is known to reconstruct into (1 × 2) in UHV[2], while both (1 × 2) and (1 × 3) in electrochemical environment have been reported.[44−46] Based on the present EC-STM studies, (1 × 3) is the only reconstructed structure observed for the Au(110) surface in NH_4Ac and phosphate buffer and in $NaClO_4/HClO_4$ solution. Representative EC-STM images are given in Figure 2A,B, showing uniform stripes that cover the whole Au(110)-electrode surface along the [1$\bar{1}$0] direction. Clear (1 × 3) elements with a periodicity of 1.30 ± 0.10 nm are observed both in neutral (26 mM NH_4Ac, pH 6.5) and acid (0.1 M $NaClO_4/HClO_4$, pH 2.5) media. This value corresponds to 3 times the nearest-neighbor distance a = 4.08 Å along the [001] direction, clearly indicative of a (1 × 3) pattern (Figure 2C). In contrast to Au(111) and Au(100), the electrochemical reconstruction of Au(110) is different from UHV environment.[2,44−46,56,57] Figure 2A,B thus exposes the local microenvironment for nucleobase adsorption which is addressed next by CV, EC-STM, and DFT computations.

Electrochemical Investigation of Assemblies of DNA Nucleobases on the Au(110) Surface. Electrochemistry offers ensemble-averaged insight in the packing and surface interactions on nucleobase adsorption, which serves as a background for molecular scale mapping by EC-STM. The electrochemical investigations of the DNA nucleobases adsorbed on the Au(110) surface were focused on the capacitive (double layer) region to avoid H_2 evolution at negative potentials and Au oxidation/reduction at positive potentials. Figure 3 summarizes cyclic voltammograms of the four bases on Au(110), compared with cyclic voltammograms of bare Au(110) in the same supporting electrolyte, $NaClO_4/HClO_4$ (pH 2.5). The pair of well-defined reconstruction peaks between 0.0 and 0.15 V vs SCE from bare Au(110) disappears in a few minutes after DNA bases are added to the electrochemical cell. This suggests that adsorption of the DNA bases on the Au(110) surface is complete within minutes, in accord with reported data for A and C adsorption at the Au(110)/electrolyte solution interface.[33,41,58] A small cathodic peak appears for A, C, and G at −0.2, −0.1, and −0.1 V, respectively, and a pair of anodic and cathodic peaks between −0.1 and −0.3 V for T. This observation is in strong contrast to voltammetric peaks for A, T, and C on Au(111) in acid supporting electrolyte, where sharp cathodic and anodic peaks

DOI: 10.1021/jp511909f
J. Phys. Chem. B 2015, 119, 3123−3134

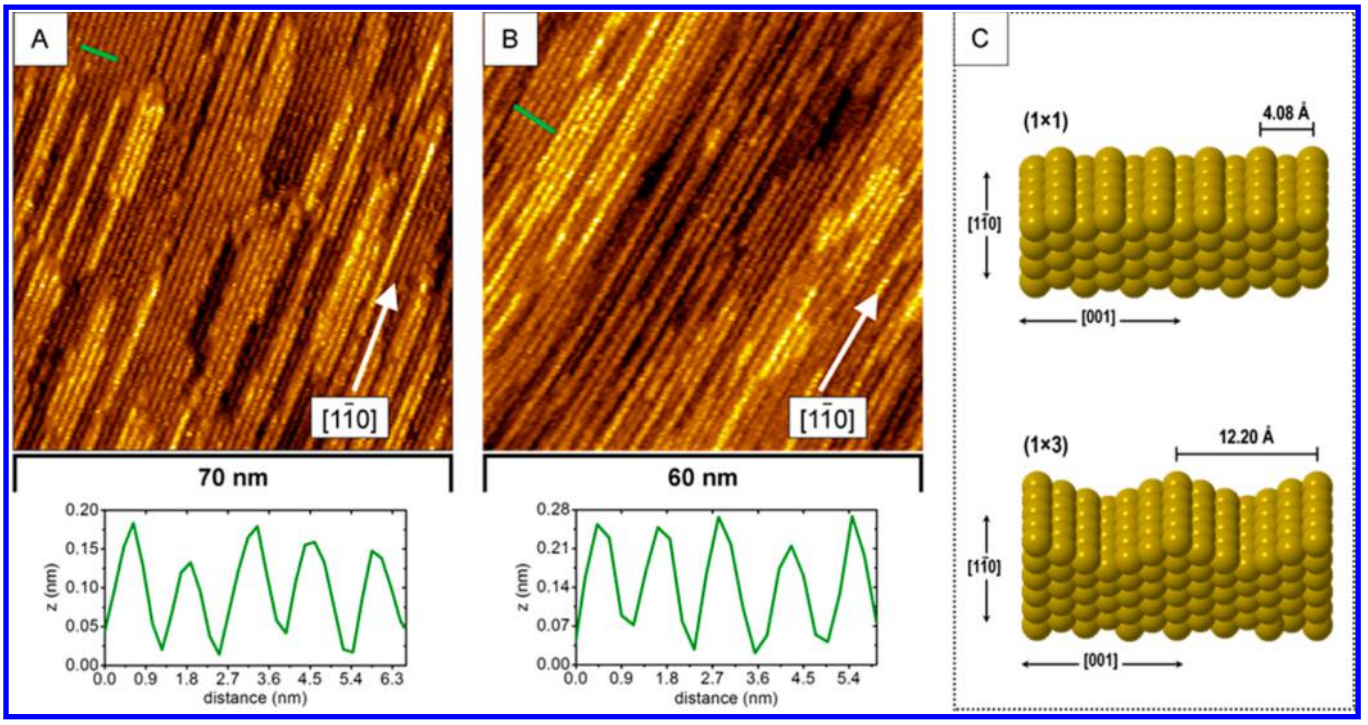

Figure 2. EC-STM images for bare Au(110)-electrode surface in (A) 26 mM NH_4Ac (pH 6.5) and (B) 0.1 M $NaClO_4/HClO_4$ (pH 2.5). (A) E_w = −0.46 V vs SCE, E_{bias} = 0.05 V. (B) E_w = −0.27 V vs SCE, E_{bias} = −0.05 V. I_{tunnel} = 35 pA. (C) Schematic drawing of (1 × 1) and (1 × 3) reconstructed Au(110)-electrode surfaces.

appear between 0.30 and 0.50 V vs SCE for C, strong but less sharp peaks at 0.0 V vs SCE for A, and needle-like capacitive peaks at 0.0 V vs SCE for T.[6,11,30,35] Such voltammetric peaks for non-redox molecules are caused by physical adsorption accompanied by potential-dependent phase transitions.[11,54] No such peaks are found for any of the four bases on Au(110) electrodes. This suggests that DNA bases added into the electrolyte solution (pH 2.5) find the way to lift the reconstruction of Au(110) and to form stable adlayers on the unreconstructed surface, most likely due to chemisorption. DFT computations reported below also support chemisorption.

EC-STM of Nucleobases on Au(110). Adsorption of the four bases on Au(110) in $NaClO_4/HClO_4$ (pH 2.5) was further studied using EC-STM to address molecular scale packing and surface interactions of the bases on the Au(110)-electrode surface. Other supporting electrolyte solutions with higher pH were also used, aiming at addressing pH effects and pH dependent solubility caused by protonation of the DNA nucleobases. Molecular structures of the DNA bases are given in Figure S2 of the Supporting Information. Table 1 gives an overview of the surface organization of the four bases at the electrolyte/Au(110) electrode interface at the three pH values addressed in this work. EC-STM-based monolayer structures of the four DNA bases assembled on Au(110) are discussed here. The computational results and a discussion of how these can support and assist the experimental image interpretation are given below.

Adenine. Monolayers of adenine on single-crystal metal surfaces such as Au(111) and Cu(110) have been investigated using different surface techniques.[4,5,11,29] Both planar orientation and vertical/tilted binding via $-NH_2$ and N7 have been reported.[31,32,36−39,59,60] Two drastically different adenine monolayer structures on Au(110) at two different pH values (Figure 4) were found in the present work. The (1 × 3) reconstruction is lifted by A adsorption in 20 mM KH_2PO_4 (pH 4.5), though residual reconstruction lines are still visible (Figure 4A,B). "Worm-like" features of 3−10 nm length cover most of the Au(110) surface and tend to align perpendicularly to the [1$\bar{1}$0] direction. These structures consist of individual 0.6−0.7 nm spaced adenine molecules in suggested upright orientation and were stable through scanning. The same organization along the [1$\bar{1}$0] direction has been observed for the Au(111) plane[4] and was attributed to $\pi-\pi$ interactions of vertically oriented A molecules.

A different surface structure is observed for A monolayers on Au(110) at lower pH. Figure 4C,D shows small (ca. 10 nm), almost planar terraces covered by a dense layer of A molecules in 0.1 M $NaClO_4/HClO_4$ (pH 2.5). No "worm-like" structures are observed. Instead, 0.8−1.0 nm ring-like structures are packed along the [001] direction, suggesting a flat orientation of A on the Au(110) surface. Repeated EC-STM scans did not produce any change neither in the worm-like nor in the flat-lying structures for potentials more positive than −0.2 V vs SCE. The different surface organization of A on the same crystallographic gold surface at two different pH values is ascribed to different protonation states of this nucleobase at pH 4.5 and 2.5. A is singly protonated at pH 2.5 ($pK_a \approx 4.2$).[61,62] An adsorption model based on DFT calculations illuminates this further and is discussed below.

Cytosine. Several different highly ordered, potential-dependent C monolayer phases on Au(111) have been reported.[6] EC-STM imaging in the present work provides evidence of only a single structure on the Au(110)-electrode surface. C molecules are adsorbed spontaneously onto Au(110) in solution at the OCP and at potentials negative of the OCP, consistent with the electrochemical behavior. The characteristic (1 × 3) reconstruction lines of Au(110) are completely lifted in the presence of a C monolayer, and small terraces formed (Figure

DOI: 10.1021/jp511909f
J. Phys. Chem. B 2015, 119, 3123−3134

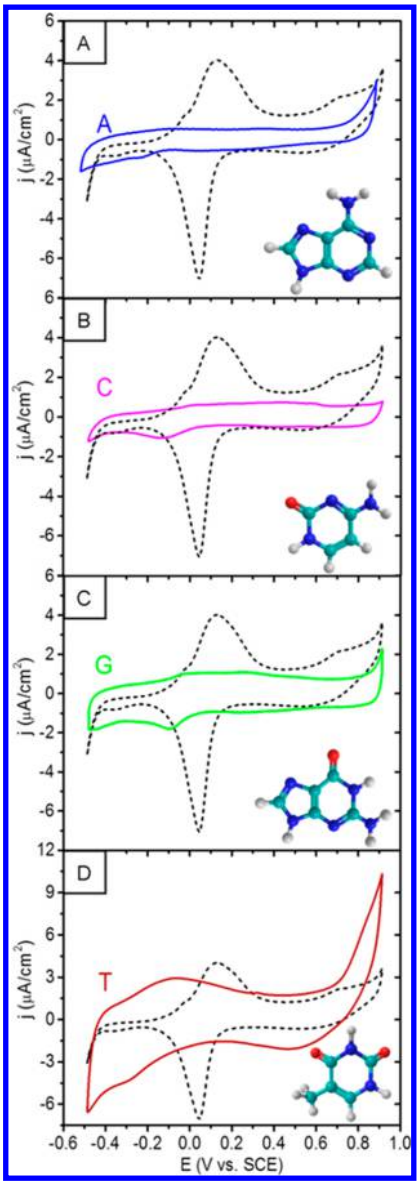

Figure 3. Cyclic voltammograms of (A) adenine (10 mM), (B) cytosine (3 mM), (C) guanine (0.4 mM), and (D) thymine (10 mM) on the Au(110)-electrode surface. 0.1 M $NaClO_4/HClO_4$ (pH 2.5). Scan rate: 50 mV s^{-1}. The dashed curve is the cyclic voltammogram of bare Au(110)-electrode surface in the same electrolyte showing the Au(110) reconstruction and lift of reconstruction. All the voltammograms were stable already after the first cycle.

Table 1. Surface Orientation of the Four DNA Nucleobases at the Au(110)/Liquid Interface at Different pH

	surface orientation at		
	pH 2.5	pH 4.5	pH 6.5
adenine	planar	vertical	
cytosine	planar		planar
guanine	disordered		vertical
thymine	planar		

5). No worm-like structures, but ordered and densely packed ring-like features appear. This suggests that C molecules adopt a flat orientation on the gold surface, in contrast to a vertical orientation of C observed on the Au(110) plane in neutral solution, independent of the potential.[12,33] This indicates that

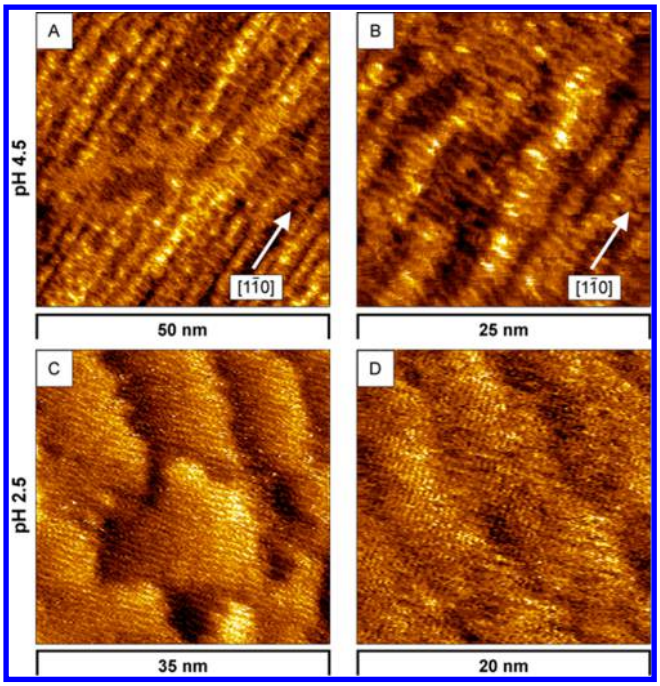

Figure 4. EC-STM images of (A, B) 0.02 mM adenine in 20 mM KH_2PO_4 (pH 4.5) and (C, D) 1.5 mM adenine in 0.1 M $NaClO_4/HClO_4$ (pH 2.5) on Au(110)-electrode surface. (A) E_{bias} = −0.25 V, E_{tip} = −0.27 V vs SCE, E_w = −0.02 V vs SCE. (B) E_{bias} = −0.50 V, E_{tip} = −0.27 V vs SCE, E_w = 0.23 V vs SCE. I_{tunnel} = 60 pA. (C) E_{bias} = −0.64 V, E_{tip} = −0.32 V vs SCE, E_w = 0.32 V vs SCE. (D) E_{bias} = −0.52 V, E_{tip} = −0.24 V vs SCE, E_w = 0.28 V vs SCE. I_{tunnel} = 35 pA.

pH significantly affects the surface molecular assembly of C. Hydrogen bonds among the C molecules are likely to stabilize the monolayer structures, although STM imaging has not reached submolecular resolution, and clear evidence cannot be provided.

Guanine. Reports of guanine adsorption on gold single-crystals are fewer than for other DNA bases.[4,5,34] One experimental challenge is the low solubility of G in acid and neutral solution (<10^{-5} M in water at neutral pH[63]). However, G dissolves easily at high pH, such as 0.1 M NaOH or KOH, according with pK_{a2} = 9.2−9.6[61,62] and negative electrostatic charge. Previous studies refer only to saturated G solutions at neutral pH.[4,5] In the present work, G was first dissolved in alkaline solution. A small portion of the basic G solution was then added to the EC-STM cell at controlled pH (*in situ* adsorption). Alternatively, the Au(110) surface was exposed to the (basic) G solution for a few hours (pre-adsorption) and then transferred into the EC-STM cell with blank supporting electrolyte at controlled pH for imaging. Figure 6A,B shows two images during G monolayer formation at pH 6.5 after *in situ* G addition. G molecules seem to align in pairs along the [1$\bar{1}$0] direction (Figure 6A). Overlayers of G on top of the (1 × 3) reconstruction lines are visible. After some minutes, G molecules form small chain-like structures by reorganization on the Au(110) surface (Figure 6B). The small chains line up perpendicularly to the [1$\bar{1}$0] direction and are stable within the double-layer region, up to 0.3 V vs SCE. The G features resemble worm-like structures on Au(111).[4] It is therefore reasonable to conclude that upright orientation dominates also in G monolayers on Au(110). Notably, a more disordered worm-like structure is disclosed at pH 2.5 (Figure 6C,D). The G monolayer structure is different from those for A and C at

DOI: 10.1021/jp511909f
J. Phys. Chem. B 2015, 119, 3123−3134

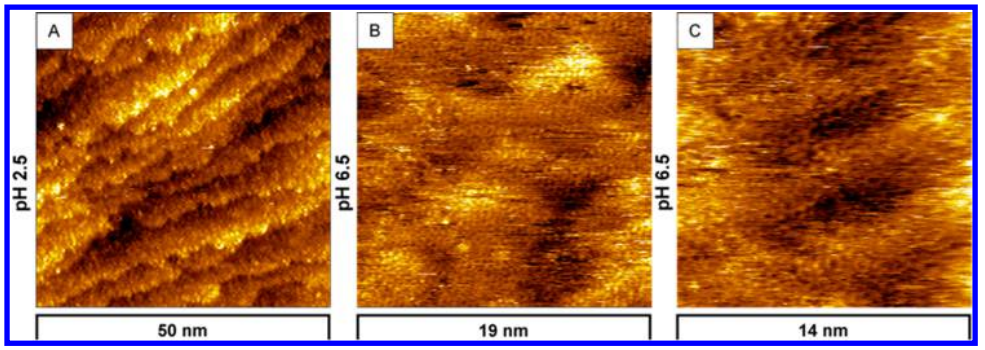

Figure 5. EC-STM images of (A) 0.5 mM cytosine in 0.1 M $NaClO_4/HClO_4$ (pH 2.5) and (B, C) 0.4 mM cytosine in 0.1 M NH_4Ac (pH 6.5), on Au(110)-electrode surface. Sample preparation: pre-adsorption. (A) E_{bias} = −0.54 V, E_{tip} = −0.12 V vs SCE, E_w = 0.42 V vs SCE. I_{tunnel} = 35 pA. (B) E_{bias} = −0.02 V, E_{tip} = −0.08 V vs SCE, E_w = −0.06 V vs SCE. I_{tunnel} = 100 pA. (C) E_{bias} = −0.02 V, E_{tip} = −0.04 V vs SCE, E_w = −0.02 V vs SCE. I_{tunnel} = 100 pA.

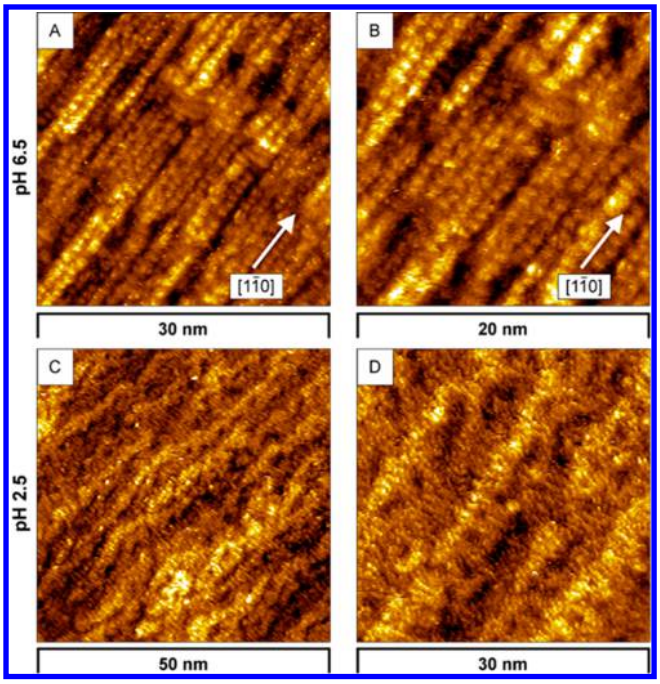

Figure 6. *In situ* STM images of (A, B) 3.7 mM guanine in 0.1 M NH_4Ac (pH 6.5) and (C, D) 0.4 mM guanine in 0.1 M $NaClO_4/HClO_4$ (pH 2.5) on Au(110)-electrode surface. (A) E_{bias} = −0.35 V, E_{tip} = −0.66 V vs SCE, E_w = −0.31 V vs SCE. (B) E_{bias} = −0.35 V, E_{tip} = −0.66 V vs SCE, E_w = −0.31 V vs SCE. I_{tunnel} = 35 pA. (C) E_{bias} = −0.49 V, E_{tip} = 0.05 V vs SCE, E_w = 0.54 V vs SCE. (D) E_{bias} = −0.44 V, E_{tip} = 0.14 V vs SCE, E_w = 0.58 V vs SCE. I_{tunnel} = 40 pA.

the same pH, but the G features were not as well resolved as the A and C adlayers. A mixture of differently oriented G molecules in the monolayers is in fact a likely conclusion for low pH. Different protonation states of G at pH 6.5 (neutral) and 2.5 (positively charged) accords with a pK_{a2} value of 9.2−9.6 and a pK_{a1} value of ≈3.4[61,62] and must therefore play a key role in the surface molecular assembly.

Thymine. T molecules on Au(110) give a pair of bump-like voltammetric peaks between −0.3 and −0.1 V vs SCE (Figure 3D), in contrast to the well-defined peaks at 0−0.15 V caused by Au(110) reconstruction/lift of reconstruction. The bump peaks also differ from the sharp potential-dependent T peaks on Au(111)[30,35] caused by phase transition in the monolayers. The nature of such bump-like peaks is not clear. In acid solution T forms dense monolayers on Au(110) resulting in large terraces (Figure 7A) and causes surface gold atoms to reorganize drastically at pH 2.5. Because of low solubility of T

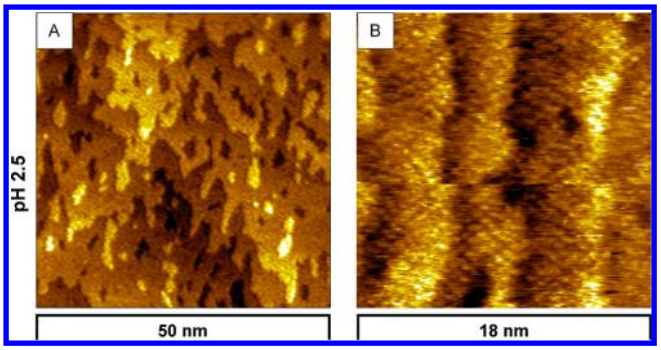

Figure 7. EC-STM images of 1.5 mM thymine in 0.1 M $NaClO_4/HClO_4$ (pH 2.5) on Au(110)-electrode surface. (A) E_{bias} = −0.31 V, E_{tip} = 0.13 V vs SCE, E_w = 0.44 V vs SCE. (B) E_{bias} = −0.75 V, E_{tip} = −0.16 V vs SCE, E_w = 0.59 V vs SCE. I_{tunnel} = 30 pA.

in neutral pH, and the fact that the quality of STM images for T at neutral pH is not high enough, only adsorption of thymine at low pH was addressed here. Similar terraces were found on thiol-bound L-cysteine monolayer formation on Au(110)-surfaces, with Au−S chemical bond formation.[3] T assemblies with many rings packed together are apparent in the double layer region up to 0.5−0.6 V vs SCE (Figure 7B). The T adsorbate layers were stable on repeated EC-STM scanning and independent of the potential. A large-magnification image shows an oblique lattice (Figure 7B), similar to previous findings for T adsorbed on Au(111).[4,30,35] This suggests that chemisorption is involved in the formation of the T adlayer on Au(110), as also reported for this nucleobase on Au(100) and Au(111) in certain potential regions.[30,35] In contrast to upright orientation recently observed by RAS on Au(110),[14] a planar T orientation is thus consistent with the EC-STM images.

The overarching view of the adsorption layer structures can be summarized in the following way. Together electrochemistry and EC-STM offer a view of the adsorption of the nucleobases on the Au(110)-electrode surface with distinct adsorption modes of the four bases. EC-STM of A and G has reached close to molecular scale resolution, while the resolution for C and T is not at this level. Still, the following hypotheses can be formulated based on the experimental data. A is adsorbed in "worm-like" bands at pH 4.5 with single molecules aligned perpendicularly to the surface by $\pi-\pi$ stacking but in ring-like

DOI: 10.1021/jp511909f
J. Phys. Chem. B 2015, 119, 3123−3134

structures with flat-lying orientation at low pH. C molecules only display ring-like structures and flat-lying orientation independent of pH. G aligns in long chains of pairs in upright orientation at high pH (6.5), while a mixture of different orientations emerges at low pH. Planar orientation in rings packed together with strong chemisorption appears, finally to be the most likely adsorption mode for thymine (pH 2.5). Upright orientation thus seems to dominate for the purine bases (A and G) and flat-lying orientation for the pyrimidine bases (C and T). These observations are summarized in Table 1. A more detailed consideration of the adsorption layers calls for molecular modeling. The preliminary conclusions (Table 1) are compared with the results of DFT computations in the next section.

DFT Calculations of Molecular Structures, Adsorption Energies, and Solvation on Au(110). First, according to the DFT calculations, bond lengths and valence angles of the nucleobases do not change significantly on adsorption. Although such calculations were started from strictly planar or vertical orientation, the plane of the adsorbed molecules emerges finally as tilted (see values of the angle between the aromatic ring and the metal surface θ in Tables S1−S3 of the Supporting Information). As the DNA bases interact with the electrode surface through molecular functional groups, the tilt angle depends on the individual DNA base molecules, being the largest for G and the smallest for C. The N atoms of the pyrimidine group (as well as the O atom of C and T) form the shortest chemical bond with the Au atoms for all the bases. Adsorption is accompanied by partial transfer of electronic charge from the molecules to the metal surface in a way that resembles coordination chemical bonding. The adsorbate charge is nearly the same for all four nucleobases being the most positive in the orientation parallel to the surface.

Second, the adsorption of the DNA bases occurs at an electrochemical interface. The adsorbed molecules can therefore displace one or more water molecules from the electrode surface. This water molecular displacement was addressed by assuming that either a single (vertical orientation of the DNA molecules) or two water molecules (the planar orientation) are displaced. An exception is cytosine, for which two water molecules were taken for both orientations due to the specific adsorption behavior of this nucleobase. Some characteristics of an adsorbed H_2O molecule are collected in Table S4. The bridge 2 (with the shortest Au−Au distance) and on-top sites with the O atom toward the metal surface were found to be the most favorable. A possible effect of anions on the adsorption of DNA bases was neglected for simplicity's sake.

Third, the metal−adsorbate bond energy in the planar orientation ΔE_{ads} ranges from 0.5 to 1.0 eV following the order G > C > A > T (Tables 2−4). This order accords with reported results of periodical DFT calculations for Au(111)[63] (C ≈ G > A > T) as well as with thermal desorption data for polycrystalline gold films.[59] However, a different order, G ≈ A > T > C, on the Au(111) surface followed from molecular dynamics (MD) simulations at low coverage.[10] The DNA base−Au interaction is therefore sensitive to the particular monocrystalline face. Planar orientation shows the largest gas phase adsorption energy (consistent with reported studies,[64] except for C with nearly the same ΔE_{ads} for both orientations). Protonated A and G show stronger interaction with the Au(110) surface in the gas phase compared with their molecular forms.

Table 2. Metal−Adsorbate Bond Energy, ΔE_{ads}, for an A Molecule and Its Protonated Form Adsorbed on the Au(110) Surface,[a] Change in Solvation Energy, $\delta\Delta E_{solv}$, of the Molecule Going from Bulk Solution to the Metal Surface,[b] and Overall Resulting Adsorption Energy, $\Delta E_{ads}^{\#}$, from Solution to the Adsorbed State[c] (Adsorption Energy from Gas Phase Corrected for $\delta\Delta E_{solv}$ and Water Desorption Energy)

	molecule		protonated form	
	planar	vertical	planar	vertical
$-\Delta E_{ads}$, eV	0.89	0.69	1.1	1.07
	0.65[d]	0.46[d]	1.2[d]	1.09[d]
	0.67[e]	0.48[e]		
$\delta\Delta E_{solv}$, eV	0.08	0.1	0.44	0.55
$-\Delta E_{ads}^{\#}$, eV	0.1	0.23	∼0	0.16

[a] $\Delta E_{ads} = E_{tot}(Au_n{-}X) - E_{tot}(Au_n) - E_{tot}(X)$, where X notes the DNA base molecule. Calculation is based on a model of the $Au_{32}(20 + 12)$ cluster from gas phase in two different orientations. [b] $\delta\Delta E_{solv} = \Delta E_{solv}(surf) - \Delta E_{solv}(bulk)$, where $\Delta E_{solv}(surf)$ is the solvation energy of the molecule adsorbed at the metal surface and $\Delta E_{solv}(bulk)$ is the same quantity calculated for bulk solution. [c] $\Delta E_{ads}^{\#} = \Delta E_{ads} + \delta\Delta E_{solv} - n\Delta E_{ads}(w)$, where $\Delta E_{ads}(w)$ is the water adsorption energy (Table S4), n is roughly 2 for planar and 1 for vertical orientation for purely geometric reasons. Cytosine with n close to 2 for both orientations is an exception. [d] The results obtained using the Au_{44} cluster. [e] The results obtained using the Au_{56} cluster.

Table 3. Metal−Adsorbate Bond Energy for a G Molecule and Its Protonated Form on the Au(110) Surface (Notations the Same as in Table 2)

	molecule		protonated form	
	planar	vertical	planar	vertical
$-\Delta E_{ads}$, eV	1.2	0.74	1.83	0.36
	0.79[a]	0.56[a]	1.71[a]	0.32[a]
	0.93[b]	0.66[b]		0.36[b]
$\delta\Delta E_{solv}$, eV	0.32	0.33	0.93	∼0
$-\Delta E_{ads}^{\#}$, eV	0.16	0.05	0.18	0

[a] The results obtained using the Au_{44} cluster. [b] The results obtained using the Au_{56} cluster.

Table 4. Metal−Adsorbate Bond Energy for C and T Molecules Adsorbed at the Au(110) Surface (Modeled by the $Au_{32}(20 + 12)$ cluster) from Gas Phase in Two Different Orientations (Corrected to the BSSE) (Notations the Same as in Tables 2 and 3)

	cytosine		thymine	
	planar	vertical	planar	vertical
$-\Delta E_{ads}$, eV	1.17	1.19	0.78	0.44
	0.94[a]	0.86[a]	0.6[a]	0.35[a]
	1.01[b]	0.98[b]		
$\delta\Delta E_{solv}$, eV	0.33	0.4	0.06	0.16
$-\Delta E_{ads}^{\#}$, eV	0.12	0.07	∼0	∼0

[a] Results obtained using the Au_{44} cluster. [b] Results obtained using the Au_{56} cluster.

Fourth, solvation affects strongly the adsorption at electrochemical interfaces. Rigorous solvent modeling requires MD simulations where the solvent molecules are explicitly included. Such an approach is very computer time demanding, and a cruder, but much faster way was used here instead. The latter

DOI: 10.1021/jp511909f
J. Phys. Chem. B 2015, 119, 3123−3134

approach rests on partial desolvation of the adsorbed bases (while maintaining the continuum model) and desorption of water molecules (see footnotes to Table 2). These corrections result in a drastic decrease of ΔE_{ads} and a change of the adsorption energy order, which is now A > G > C > T, ranging from ≈0.2 eV for A in vertical orientation to ≈0 eV for T in planar orientation (Tables 2−4). This accords with reported experimental RAS data for A adsorption at the Au(110)/electrolyte solution interface.[58] From the adsorption energies vertical orientation for A thus seems robust, and flat orientation remains the most favorable for G and C molecules. Notably, however, the adsorption energy differences between the different orientations (vertical, flat-lying) with solvation effects and water molecular desorption included is small and only varies by about a tenth of an electronvolt. Adsorbate intermolecular surface interactions are therefore expected to be important. The small adsorption energy differences would also lead both to the presence of a mixture of two orientations as seen for G and to fast interconversion between different equilibrium adsorbate orientations. This outcome of the DFT computations therefore also offers one immediate clue to the limited EC-STM image resolution ("blurred" images) observed.

So far the adsorption of only a single molecule was addressed. Intermolecular H-bonds between adsorbed DNA bases are, however, known to be crucial in monolayer formation on gold surfaces.[10] The normal ($\mu_\perp$) and longitudinal (μ_P) projections of the total dipole moment of the DNA base molecules were calculated using their geometry in the adsorbed state (Table S5). From a qualitative viewpoint, it is clear that the higher $\mu_\perp$, the stronger is the Coulomb repulsion between adsorbed molecules. For a certain surface lattice, on the other hand, a larger μ_P results in significant electrostatic attraction between the dipoles. Dipole−dipole interactions favor planar orientation for A, G, and C molecules, while planar and tilted orientations might be equally likely for T (Table S5).

Computed EC-STM Contrasts. The STM contrasts (constant current mode) were calculated in the framework of the quantum chemical model previously developed.[3,65] STM electron transfer (ET) was treated as a bridge-assisted superexchange process in which ET from adsorbate to the metal surface is adiabatic, whereas the adsorbate/STM tip transition is diabatic. The STM tip was represented by a tungsten atom. The optimized geometry of the adsorbed nucleobases was used (Figures S3−S8). The influence of the metal surface was not addressed directly. In the diabatic weak-coupling limit of tip−molecule interaction, the tunneling current is proportional to the squared electronic coupling factor V_{if} (resonance integral). The latter was calculated in terms of two-level perturbation theory.[3,65] Also, comparison of the model STM contrasts is more convenient (visually), if the difference between the calculated image heights for different nucleobases and their orientations are kept within a narrow interval. This is why different values for the electronic coupling factor were used (Figures S3−S8). The V_{if} values for the molecules in planar orientation correspond to notably adiabatic ET between the STM tip and the adsorbed molecule, while the ET for vertical orientation was assumed to be diabatic.

The computed images are, first, significantly different for planar and vertical orientations (Figures S3−S8) and clearly distinctive with respect to these orientations. Together with the computed adsorption energies, the computed contrasts therefore offer a rationale for the observed EC-STM contrasts. Notably, the "planar" tunneling contrasts of nonprotonated A and T demonstrate submolecular resolution, whereas the "vertical" contrasts do not. Second, the protonation of the A and G molecules adsorbed in planar orientation clearly decreases the submolecular level of model contrast resolution. Third, the computed contrasts notably exceed the size of the molecules with significant electronic contrast (electronic density "spillover") beyond the molecular frame. This adds an additional clue to the apparently blurred nature of the images. The distinct appearance of the computed images for different adsorbate orientations finally offers direct insight into the physical nature of the binding modes, at least for A and G, for which the observed EC-STM resolution is highest and close to molecular scale resolution. As follows from these studies, the aromatic rings give a significant contribution to the highest occupied molecular orbital of A and G, which is why the angle between the ring and metal surface is small (Tables S1 and S2). Moreover, for both orientations of A and G the N atom from the pyridine group (N_2) contributes noticeably to the chemical bond with the metal, as judged from the shortest Au−N_2 bond length values in comparison with other atoms.

■ CONCLUSIONS

The present study, based on CV, EC-STM, and electronic structure computations, shows first that the four DNA bases are strongly adsorbed on Au(110)-electrode surfaces, both at the OCP and under electrochemical control in a wide potential range, indicative that chemisorption is the prevailing mode. Chemisorption is accompanied by lifting of the (1 × 3) reconstruction of Au(110). The monolayers are stable and independent of potential in a wide potential range. This is in striking contrast to physical adsorption of the same molecules on Au(111) surfaces on which different potential dependent monolayer phases are formed.

Close to molecular EC-STM resolution has, second, been achieved for A and G monolayers and a striking pH-dependence of A and G packing observed. The (1 × 3) reconstruction is lifted on A adsorption at pH 4.5, though residual reconstruction lines remain (Figure 4A,B) after addition of A molecules into the STM cell. 3−10 nm "worm-like" features aligned perpendicularly to the [1$\bar{1}$0] direction cover most of the Au(110) surface. These structures consist of stable individual 0.7 nm spaced A molecules of suggested upright orientation. The same organization is reported for Au(111)[4] and attributed to $\pi-\pi$ interactions of vertically oriented A molecules. A different surface structure is observed for A monolayers at low pH (2.5), where small (ca. 10 nm) terraces covered by a dense layer of A molecules appear (Figure 4C,D). No "worm-like", but 0.8−1.0 nm ring-like structures are packed along the [001] direction. These are stable and suggest a flat orientation. The different surface organization of A on the same crystallographic gold surface orientation is ascribed to protonation of A. Minimal intermolecular electrostatic repulsion of the protonated form is probably ensured in the flat-lying orientation.

The low solubility of G in acid and neutral solution (<10^{-5} M) is an issue, but G dissolves easily at high pH. Following the procedure above, EC-STM imaging at pH 6.5 with molecular scale resolution could be achieved (Figure 6A,B), although not as well resolved as for A. G molecules align in pairs along the [1$\bar{1}$0] direction (Figure 6A). After some minutes, the G molecules reorganize into small chain-like structures (Figure 6B), consistently lined up perpendicularly to the [1$\bar{1}$0] direction, up to 0.3 V vs SCE. The G features resemble the

DOI: 10.1021/jp511909f
J. Phys. Chem. B 2015, 119, 3123−3134

"worm-like" structures formed by A and G on Au(111)[4] and by A on Au(110). It is therefore concluded that upright G orientation prevails at pH 6.5. More disordered worm-like structures appear at pH 2.5 (Figure 6C,D). These differ from those of both A and C on Au(110) at the same pH. A mixture of differently oriented G molecules is the most likely conclusion. Indeed, the computed difference in the adsorption of G from solution is small for the two different orientations (Table 3); lateral electrostatic interactions in the monolayer may favor flat orientation (Table S5).

No pH dependence of C monolayer packing was found. Several highly ordered, potential-dependent C monolayer phases on Au(111) have been reported,[6] but EC-STM imaging in the present work has provided evidence of only a single structure on the Au(110) plane. C monolayer formation causes the (1 × 3) Au(110) reconstruction lines to lift completely and small terraces to be formed (Figure 5). No worm-like structures, but ordered densely packed ring-like features, appear, suggesting that C molecules adopt a flat-lying orientation. This agrees with the computational predictions (Table 4). The same patterns are seen in acid and neutral solutions, meaning that protonation of C is unimportant. STM features of C monolayers were not resolved to the molecular scale, but hydrogen bonds among the C molecules are likely to stabilize the monolayer structures, as noted from RAS studies.[33]

Finally, T molecules form dense monolayers resulting in large terraces (Figure 7A), indicative of drastic reorganization of the surface Au atoms at pH 2.5. Similar terraces were found on thiol-bound L-cysteine monolayer formation on Au(110).[3] T structures with some sort of ring-like structures packed together are apparent in the double-layer region up to 0.5−0.6 V (Figure 7B). The rings are stable on repeated EC-STM scanning, and independent of the potential applied, and form an oblique lattice, similar to previous findings for T on Au(111).[4,30,35] This suggests that T is chemisorbed on Au(110), similarly to T adsorption on Au(100) and Au(111).[30,35] On the basis of the present work, flat-lying T orientation is likely at pH 2.5, although this conclusion is in contrast to upright orientation suggested by RAS on Au(110) at neutral pH.[14] Such a different surface molecular assembly of T can be attributed to a difference in pH. As follows from the DFT calculations, the adsorption of a T molecule from bulk solution is, however, very weak for both orientations (Table 4), so that the main factor in the stabilization of cluster structures of adsorbed T molecules must be hydrogen bonds and other intermolecular lateral electrostatic interactions (Table 4).

The four bases thus bind in different chemisorption modes. Binding of the purine bases (A and G) depends furthermore strongly on pH. "Worm-like" alignment of upright oriented molecules dominates at high pH for both A (pH 4.5) and G (pH 6.5). The rows are organized in individual row structures for A, but in pairs for G. The organization is different for A and G at low pH (2.5), where both bases are protonated. Flat-lying A molecules assemble in rings on small terraces, while G molecules pack in a mixture of flat-lying and upright stacked orientations. The pyrimidine bases (C and T) are chemisorbed in flat-lying orientations parallel to the Au(110) surface, independently of pH. Chirality may accompany chemisorption on the Au(110) surface as observed for A on Cu(110) in UHV,[29] but the EC-STM resolution presently is insufficient for distinction between different enantiomeric forms.

The DFT computations broadly support the observed binding modes for A and G, i.e. both bases are significantly chemisorbed and the dominating vertical binding of A is also the orientation of highest binding energy. The binding energy of G is approximately the same in both orientations according with the observed presence of both in the EC-STM images. The DFT support is less conclusive for C and T for both of which the binding energy is very small and intramolecular and other forces dominate the packing. In addition, the following computational outcomes and conceptual bridges to the electrochemical and EC-STM data are particularly noted.

- Subtle interactions between the nucleobases and the Au(110)-substrate, intermolecular interactions among the chemisorbed nucleobase molecules, and solvation effects are all crucially involved. The different observed base specific chemisorption modes and the "fuzzy" appearance of the EC-STM images suggest that the three kinds of forces are of comparable strength. The DFT computations hold clues to the direct chemisorption of the individual nucleobase molecules and the solvation effects, as well as to the intermolecular adsorbate interactions, as reflected in the observed base specific EC-STM images.
- Substantial charge transfer from adsorbate molecule to the electrode surface (cluster) accompanies adsorption, indicative of strong chemisorption (Tables S1−S3 in the Supporting Information).
- The direct adsorption energy of an A molecule in the gas phase is more favorable for planar (flat-lying) orientation than for upright orientation (Table 2), but this is more than compensated by the more favorable solvation (free) energy giving overall more favorable upright than flat-lying A orientation, as observed from EC-STM. This conclusion applies to protonated A as well. The total chemisorption free energy differences are, however, small (i.e., 13−160 meV), strongly suggesting the importance of fast interconversion between different orientations and therefore "fuzzy" images.
- Solvation is also highly important for G chemisorption, but with the opposite outcome, i.e., flat-lying orientation is the more favorable. As the chemisorption free energy is still small (i.e., 110−180 meV) in both orientations, it is, however, understandable that both flat-lying and upright G orientation can be present simultaneously, consistent with the EC-STM images.
- The total chemisorption free energies of the flat-lying and upright orientations are almost the same for C and T, i.e., both <50 meV (Table 4). The EC-STM images suggest that flat-lying orientation dominates in both cases, but the small adsorption free energy and the "fuzzy" image character suggest again that multiple orientations with fast interconversion are present.

Broad consistency between the multifarious chemisorption modes of the four nucleobases observed by EC-STM and the DFT computations thus emerges.

As a final note, adsorption of DNA bases follows other cases of strong non-thiol-based molecular adsorption. Structure and dynamics of SAMs based on Au−S bond formation offer prodigious approaches to molecular architecture and functional nanomaterials.[25,58,66,67] These have been studied extensively by a number of *in situ* techniques, but other adsorption modes to form stable monolayers have been searched. For example, the non-thiol molecule, triazatriangulenium (TATA) ion, can assemble on Au(111) and be combined with other functional groups by chemical synthesis.[68] The present work shows that biological molecules that adsorb weakly by physical adsorption on smooth single-crystal Au(111)-surfaces can form stable

DOI: 10.1021/jp511909f
J. Phys. Chem. B 2015, 119, 3123−3134

monolayers by chemisorption on Au(110). This means that broad varieties of non-thiol bound molecules can in fact form stable monolayers on the (110) surface, also when no stable monolayers of the molecules form on Au(111) surfaces.

Intermolecular interactions between the adsorbed species were only considered qualitatively in this work. More rigorous monolayer models of adsorbed DNA species remain a major challenge for forthcoming computational studies. Such models would address both short-range H-bonds and long-range electrostatic interactions and enable predicting nucleobase cluster structures at the electrode surface. A challenge in forthcoming experimental work would be particularly to attain better STM image resolution of individual adsorbate molecules.

■ ASSOCIATED CONTENT

Supporting Information

Computed water molecular orientations; molecular structures and properties of DNA nucleobases; adsorption bond and orientation parameters for the four nucleobases; simulated STM images for the four DNA bases. This material is available free of charge via the Internet at http://pubs.acs.org.

■ AUTHOR INFORMATION

Corresponding Author

*(J.Z.) Phone +45 45252352; Fax +45 45883136; e-mail jz@kemi.dtu.dk.

Present Address

P.S.: Istituto Italiano di Tecnologia, Smart Materials - Nanophysics Department, Via Morego 30, 16163 Genoa, Italy.

Notes

The authors declare no competing financial interest.

■ ACKNOWLEDGMENTS

This work was financially supported by the Villum Kann Rasmussen Foundation (95-305-13667VKR), the Lundbeck Foundation (R69-A8097), the Danish Research Council for Nature and Universe (12-125966), and the Russian Foundation for Basic Research (14-03-00935a).

■ REFERENCES

(1) Zhang, J.; Chi, Q.; Nielsen, J. U.; Friis, E. P.; Andersen, J. E. T.; Ulstrup, J. Two-dimensional Cysteine and Cystine Cluster Networks on Au (111) Disclosed by Voltammetry and in Situ Scanning Tunneling Microscopy. *Langmuir* **2000**, *16*, 7229−7237.

(2) Kühnle, A.; Linderoth, T. R.; Hammer, B.; Besenbacher, F. Chiral Recognition in Dimerization of Adsorbed Cysteine Observed by Scanning Tunnelling Microscopy. *Nature* **2002**, *415*, 891−893.

(3) Zhang, J.; Chi, Q.; Nazmutdinov, R. R.; Zinkicheva, T. T.; Bronshtein, M. D. Submolecular Electronic Mapping of Single Cysteine Molecules by in Situ Scanning Tunneling Imaging. *Langmuir* **2009**, *25*, 2232−2240.

(4) Tao, N. J.; DeRose, J. A.; Lindsay, S. M. Self-assembly of Molecular Superstructures Studied by in Situ Scanning Tunneling Microscopy: DNA Bases on Gold (111). *J. Phys. Chem.* **1993**, *97*, 910−919.

(5) Boland, T.; Ratner, B. D. Two-Dimensional Assembly of Purines and Pyrimidines on Au(111). *Langmuir* **1994**, *10*, 3845−3852.

(6) Wandlowski, T.; Lampner, D.; Lindsay, S. M. Structure and Stability of Cytosine Adlayers on Au(111): an in-Situ STM Study. *J. Electroanal. Chem.* **1996**, *404*, 215−226.

(7) Hölzle, M. H.; Wandlowski, T.; Kolb, D. M. Structural Transitions in Uracil Adlayers on Gold Single Crystal Electrodes. *Surf. Sci.* **1995**, *335*, 281−290.

(8) Dretschkow, T.; Dakkouri, A. S.; Wandlowski, T. In-Situ Scanning Tunneling Microscopy Study of Uracil on Au(111) and Au(100). *Langmuir* **1997**, *13*, 2843−2856.

(9) Xu, W.; Kelly, R. E. A.; Otero, R.; Schöck, M.; Lægsgaard, E.; Stensgaard, I.; Kantorovich, L. N.; Besenbacher, F. Probing the Hierarchy of Thymine−Thymine Interactions in Self-Assembled Structures by Manipulation with Scanning Tunneling Microscopy. *Small* **2007**, *3*, 2011−2014.

(10) Maleki, A.; Alavi, S.; Najafi, B. Molecular Dynamics Simulation Study of Adsorption and Patterning of DNA Bases on the Au (111) Surface. *J. Phys. Chem. C* **2011**, *115*, 22484−22494.

(11) Vaz-Dominguez, C.; Escudero-Escribano, M.; Cuesta, A.; Prieto-Dapena, F.; Cerrillos, C.; Rueda, M. Electrochemical STM Study of the Adsorption of Adenine on Au(111) Electrodes. *Electrochem. Commun.* **2013**, *35*, 61−64.

(12) Weightman, P.; Dolan, G. J.; Smith, C. I.; Cuquerella, M. C.; Almond, N. J.; Farrell, T.; Fernig, D. G.; Edwards, C.; Martin, D. S. Orientation of Ordered Structures of Cytosine and Cytidine 5′-Monophosphate Adsorbed at Au(110)/Liquid Interfaces. *Phys. Rev. Lett.* **2006**, *96*, 086102.

(13) Bowfield, A.; Smith, C. I.; Mansley, C. P.; Weightman, P. The Influence of pH on the Structure of Adenine Monolayers Adsorbed at Au(110)/Electrolyte Interfaces. *Phys. Status Solidi B* **2010**, *247*, 1937−1940.

(14) Molina Contreras, J. R.; Smith, C. I.; Bowfield, A.; Tillner, F.; Weightman, P. The Self Assembly of Thymine at Au(110)/Liquid Interfaces. *Phys. Status Solidi B* **2012**, *249*, 1−4.

(15) Zhang, J.; Kuznetsov, A. M.; Medvedev, I. G.; Chi, Q.; Albrecht, T.; Jensen, P. S.; Ulstrup, J. Single-Molecule Electron Transfer in Electrochemical Environments. *Chem. Rev.* **2008**, *108*, 2737−2791.

(16) Leger, C.; Elliott, S. J.; Hoke, K. R.; Jeuken, L. J. C.; Jones, A. K.; Armstrong, F. A. Enzyme Electrokinetics: Using Protein Film Voltammetry To Investigate Redox Enzymes and Their Mechanisms. *Biochemistry* **2003**, *42*, 8653−8662.

(17) Malvankar, N. S.; Yalcin, S. E.; Tuominen, M. T.; Lovley, D. R. Visualization of Charge Propagation along Individual Pili Proteins Using Ambient Electrostatic Force Microscopy. *Nat. Nanotechnol.* **2014**, DOI: 10.1038/NNANO.2014.236.

(18) Genereux, J. C.; Barton, J. K. Mechanisms for DNA Charge Transport. *Chem. Rev.* **2010**, *110*, 1642−1662.

(19) Kawai, K.; Hayashi, M.; Majima, T. HOMO Energy Gap Dependence of Hole-Transfer Kinetics in DNA. *J. Am. Chem. Soc.* **2012**, *134*, 9406−9409.

(20) Salvatore, P.; Zeng, D.; Karlsen, K. K.; Chi, Q.; Wengel, J.; Ulstrup, J. Electrochemistry of Single Metalloprotein and DNA-Based Molecules at Au(111) Electrode Surfaces. *ChemPhysChem* **2013**, *14*, 2101−2111.

(21) Salvatore, P.; Karlsen, K. K.; Hansen, A. G.; Zhang, J.; Nichols, R. J.; Ulstrup, J. Polycation Induced Potential Dependent Structural Transitions of Oligonucleotide Monolayers on Au(111)-Surfaces. *J. Am. Chem. Soc.* **2012**, *134*, 19092−19098.

(22) Slinker, J. D.; Muren, N. B.; Renfrew, S. E.; Barton, J. K. DNA Charge Transport over 34 nm. *Nat. Chem.* **2011**, *3*, 228−233.

(23) Sontz, P. A.; Muren, N. B.; Barton, J. K. DNA Charge Transport for Sensing and Signaling. *Acc. Chem. Res.* **2012**, *45*, 1792−1800.

(24) Katz, E.; Willner, I. Integrated Nanoparticle−Biomolecule Hybrid Systems: Synthesis, Properties, and Applications. *Angew. Chem., Int. Ed.* **2004**, *43*, 6042−6108.

(25) Zhang, J.; Welinder, A. C.; Chi, Q.; Ulstrup, J. Electrochemically Controlled Self-assembled Monolayers Characterized with Molecular and Sub-molecular Resolution. *Phys. Chem. Chem. Phys.* **2011**, *13*, 5526−5545.

(26) Zhang, J.; Chi, Q.; Hansen, A. G.; Jensen, P. S.; Salvatore, P.; Ulstrup, J. Interfacial Electrochemical Electron Transfer in Biology − Towards the Level of the Single Molecule. *FEBS Lett.* **2012**, *586*, 526−535.

(27) Bowfield, A.; Smith, C. I.; Cuquerella, M. C.; Farrell, T.; Fernig, D. G.; Edwards, C.; Weightman, P. Reflection Anisotropy Spectros-

DOI: 10.1021/jp511909f
J. Phys. Chem. B 2015, 119, 3123−3134

copy of Decanethiol Adsorbed at Au(110)/Liquid Interfaces. *Phys. Status Solidi C* **2008**, *5*, 2600−2603.
(28) Welinder, A. C.; Zhang, J.; Steensgaard, D. B.; Ulstrup, J. Adsorption of Human Insulin on Single-Crystal Gold Surfaces Investigated by in Situ Scanning Tunnelling Microscopy and Electrochemistry. *Phys. Chem. Chem. Phys.* **2010**, *12*, 9999−10011.
(29) Chen, Q.; Frankel, D. J.; Richardson, N. V. Self-Assembly of Adenine on Cu(110) Surfaces. *Langmuir* **2002**, *18*, 3219−3225.
(30) Roelfs, B.; Bunge, E.; Schröter, C.; Solomun, T.; Meyer, H.; Nichols, R. J.; Baumgärtel, H. Adsorption of Thymine on Gold Single-Crystal Electrodes. *J. Phys. Chem. B* **1997**, *101*, 754−765.
(31) Lukas, M.; Kelly, R. E. A.; Kantorovich, L. N.; Otero, R.; Xu, W.; Laegsgaard, E.; Stensgaard, I.; Besenbacher, F. Adenine Monolayers on the Au(111) Surface: Structure Identification by Scanning Tunneling Microscopy Experiment and *ab initio* Calculations. *J. Chem. Phys.* **2009**, *130*, 024705.
(32) Kelly, R. E. A.; Xu, W.; Lukas, M.; Otero, R.; Mura, M.; Lee, Y.-J.; Lægsgaard, E.; Stensgaard, I.; Kantorovich, L. N.; Besenbacher, F. An Investigation into the Interactions Between Self-Assembled Adenine Molecules and a Au(111) Surface. *Small* **2008**, *4*, 1494−1500.
(33) Mansley, C. P.; Smith, C. I.; Bowfield, A.; Fernig, D. G.; Edwards, C.; Weightman, P. Prevention of Surface Reconstruction at the Au(110)/Electrolyte Interface by the Adsorption of Cytosine. *J. Chem. Phys.* **2010**, *132*, 214708.
(34) Steenken, S. Purine Bases, Nucleosides, and Nucleotides: Aqueous Solution Redox Chemistry and Transformation Reactions of Their Radical Cations and e^- and OH Adducts. *Chem. Rev.* **1989**, *89*, 503−520.
(35) Haiss, W.; Roelfs, B.; Port, S. N.; Bunge, E.; Baumgärtel, H.; Nichols, R. J. In-Situ Infrared Spectroscopic Studies of Thymine Adsorption on a Au(111) Electrode. *J. Electroanal. Chem.* **1998**, *454*, 107−113.
(36) Prado, C.; Prieto, F.; Rueda, M.; Feliu, J.; Aldaz, A. Adenine Adsorption on Au(111) and Au(100) Electrodes: Characterisation, Surface Reconstruction Effects and Thermodynamic Study. *Electrochim. Acta* **2007**, *52*, 3168−3180.
(37) Xiao, Y.-J.; Chen, Y.-F.; Gao, X.-X. Comparative Study of the Surface Enhanced Near Infrared Raman Spectra of Adenine and NAD^+ on a Gold Electrode. *Spectrochim. Acta, Part A* **1999**, *55*, 1209−1218.
(38) Rodes, A.; Rueda, M.; Prieto, F.; Prado, C.; Feliu, J. M.; Aldaz, A. Adenine Adsorption at Single Crystal and Thin-Film Gold Electrodes: An In Situ Infrared Spectroscopy Study. *J. Phys. Chem. C* **2009**, *113*, 18784−18794.
(39) Camargo, A. P. M.; Baumgärtel, H.; Donner, C. Adsorption Behaviour of DNA Bases at the Au(111) Electrode. *PhysChemComm* **2002**, *5*, 151−157.
(40) Nichols, R. J.; Haiss, W.; Fernig, D. G.; van Zalinge, H.; Schiffrin, D. J.; Ulstrup, J. In Situ STM Studies of Immobilized Biomolecules at the Electrode-Electrolyte Interface. In *Bioinorganic Electrochemistry*; Hammerich, O., Ulstrup, J., Eds.; Springer: Dordrecht, 2008; pp 207−247.
(41) Bowfield, A.; Smith, C. I.; Dolan, G. J.; Cuquerella, M. C.; Mansley, C. P.; Weightman, P. The Structure of Adenine Adsorbed at Sub-Saturation Coverage at Au(110)/Electrolyte Interfaces. *e-J. Surf. Sci. Nanotechnol.* **2009**, *7*, 225−229.
(42) Ocko, B. M.; Helgesen, G.; Schardt, B.; Wang, J.; Hamelin, A. Charge Induced (1 × 3) Reconstruction of the Au(110) Surface: An X-ray Scattering Study. *Phys. Rev. Lett.* **1992**, *69*, 3350−3353.
(43) Gao, X.; Edens, G. J.; Hamelin, A.; Weaver, M. J. Charge-dependent Atomic-scale Structures of High-Index and (110) Gold Electrode Surfaces as Revealed by Scanning Tunneling Microscopy. *Surf. Sci.* **1994**, *318*, 1−20.
(44) Magnussen, O. M.; Wiechers, J.; Behm, R. J. In Situ Scanning Tunneling Microscopy Observations of the Potential-Dependent (1 × 2) Reconstruction on Au(110) in Acidic Electrolytes. *Surf. Sci.* **1993**, *289*, 139−151.
(45) Gao, X.; Hamelin, A.; Weaver, M. J. Reconstruction at Ordered Au(110)-Aqueous Interfaces as Probed by Atomic-resolution Scanning Tunneling Microscopy. *Phys. Rev. B* **1991**, *44*, 10983−10986.
(46) Michaelis, R.; Kolb, D. M. On the Stability of Au(110)-(1 × 2) and -(1 × 3) Reconstructed Surfaces in Contact with an Aqueous Solution. *Surf. Sci. Lett.* **1990**, *234*, L281−L284.
(47) Sowerby, S. J.; Heckl, W. M.; Petersen, G. B. Chiral Symmetry Breaking during the Self-Assembly of Monolayers from Achiral Purine Molecules. *J. Mol. Evol.* **1996**, *43*, 419−424.
(48) Sowerby, S. J.; Heckl, W. M. The Role of Self-Assembled Monolayers of the Purine and Pyrimidine Bases in the Emergence of Life. *Origins Life Evol. Biosphere* **1998**, *28*, 283−310.
(49) Hamelin, A. Cyclic Voltammetry at Gold Single-Crystal Surfaces. Part I. Behaviour at Low-Index Faces. *J. Electroanal. Chem.* **1996**, *407*, 1−11.
(50) Hamelin, A.; Stoicoviciu, L. Study of Gold Low-Index Faces in KPF_6 Solutions: Part II. Analysis of the Experimental Results. *J. Electroanal. Chem.* **1987**, *236*, 267−281.
(51) Frisch, M. J.; Trucks, G. W.; Schlegel, H. B.; Scuseria, G. E.; Robb, M. A.; Cheeseman, J. R.; Scalmani, G.; Barone, V.; Mennucci, B.; Petersson, G. A.; et al. *Gaussian 09, Revision B.01*; Gaussian, Inc.: Wallingford, CT, 2010.
(52) Liu, W.; Ruiz, V. G.; Zhang, G.-X.; Santra, B.; Ren, X.; Scheffler, M.; Tkachenko, A. Structure and Energetics of Benzene Adsorbed on Transition-metal Surfaces: Density-Functional Theory with van der Waals Interactions Including Collective Substrate Response. *New J. Phys.* **2013**, *15*, 053046.
(53) Ivaništšev, V.; Nazmutdinov, R. R.; Lust, E. A Comparative DFT Study of the Adsorption of H_2O Molecules at Bi, Hg, and Ga Surfaces. *Surf. Sci.* **2013**, *609*, 91−99.
(54) Hay, P. J.; Wadt, W. R. *Ab Initio* Effective Core Potentials for Molecular Calculations. Potentials for K to Au Including the Outermost Core Orbitals. *J. Chem. Phys.* **1985**, *82*, 270−283.
(55) Foster, J. P.; Weinhold, F. Natural Hybrid Orbitals. *J. Am. Chem. Soc.* **1980**, *102*, 7211−7218.
(56) Gao, X.; Hamelin, A.; Weaver, M. J. Atomic Relaxation at Ordered Electrode Surfaces Probed by Scanning Tunneling Microscopy: Au(111) in Aqueous Solution Compared with Ultrahigh-Vacuum Environments. *J. Chem. Phys.* **1991**, *95*, 6993−6996.
(57) Gao, X.; Hamelin, A.; Weaver, M. J. Elucidating Complex Surface Reconstructions with Atomic-Resolution Scanning Tunneling Microscopy: Au (100)-Aqueous Electrochemical Interface. *Phys. Rev. B* **1992**, *46*, 7096−7102.
(58) Smith, C. I.; Bowfield, A.; Dolan, G. J.; Cuquerella, M. C.; Mansley, C. P.; Fernig, D. G.; Edwards, C.; Weightman, P. Determination of the Structure of Adenine Monolayers Adsorbed at Au(110)/Electrolyte Interfaces Using Reflection Anisotropy Spectroscopy. *J. Chem. Phys.* **2009**, *130*, 044702−044710.
(59) Demers, L. M.; Östblom, M.; Zhang, H.; Jang, N.-H.; Liedberg, B.; Mirkin, C. A. Thermal Desorption Behavior and Binding Properties of DNA Bases and Nucleosides on Gold. *J. Am. Chem. Soc.* **2002**, *124*, 11248−11249.
(60) Martins, A.; Queirós, A.; Silva, F. Surface-Structure-Sensitive Adsorption of Adenine on Gold Electrodes. *ChemPhysChem* **2005**, *6*, 1056−1060.
(61) Lide, D. R. *CRC Handbook of Chemistry and Physics*, 80th ed.; CRC Press: Boca Raton, FL, 1999−2000.
(62) Verdolino, V.; Cammi, R.; Munk, B. H.; Schlegel, H. B. Calculation of p*K* Values of Nucleobases and the Guanine Oxidation Products Guanidinohydantoin and Spiroiminodihydantoin using Density Functional Theory and a Polarizable Continuum Model. *J. Phys. Chem. B* **2008**, *112*, 16860−16873.
(63) DeVoe, H.; Wasik, S. P. Aqueous Solubilities and Enthalpies of Solution of Adenine and Guanine. *J. Solution Chem.* **1984**, *13*, 51−60.
(64) Piana, S.; Bilic, A. The Nature of the Adsorption of Nucleobases on the Gold [111] Surface. *J. Phys. Chem. B* **2006**, *110*, 23467−23471.
(65) Nazmutdinov, R. R.; Zhang, J.; Zinkicheva, T. T.; Manyurov, I. R.; Ulstrup, J. Adsorption and In Situ Scanning Tunneling Microscopy of Cysteine on Au(111): Structure, Energy, and Tunneling Contrasts. *Langmuir* **2006**, *22*, 7556−7567.

DOI: 10.1021/jp511909f
J. Phys. Chem. B 2015, 119, 3123−3134

(66) Love, J. C.; Estroff, L. A.; Kriebel, J. K.; Nuzzo, R. G.; Whitesides, G. M. Self-Assembled Monolayers of Thiolates on Metals as a Form of Nanotechnology. *Chem. Rev.* **2005**, *105*, 1103−1170.
(67) Baisch, B.; Raffa, D.; Jung, U.; Magnussen, O. M.; Nicolas, C.; Lacour, J.; Kubitschke, J.; Herges, R. Mounting Freestanding Molecular Functions onto Surfaces: The Platform Approach. *J. Am. Chem. Soc.* **2009**, *131*, 442−443.
(68) Kuhn, S.; Baisch, B.; Jung, U.; Johannsen, T.; Kubitschke, J.; Herges, R.; Magnussen, O. Self-assembly of Triazatriangulenium-based Functional Adlayers on Au(111) Surfaces. *Phys. Chem. Chem. Phys.* **2010**, *12*, 4481−4487.

DOI: 10.1021/jp511909f
J. Phys. Chem. B 2015, 119, 3123−3134